OPEN ACCESS

REGULAR ARTICLE

Zinc Oxide Poly Crystals Heterojunction and Infrared- Blind UV-Photodetector

Saif Khalel Jasim[1,2], Ahmed M. Shano[2,*] ✉, Suzan K. Adnan[1]

[1] *Ministry of Education, Diyala Education Directorate, Diyala, Iraq*
[2] *Department of Radiological Tech., Bilad Alrafidain University College, 32001 Diyala, Iraq*

In this work, we used electrochemical etching of *p*-type silicon wafers for 10 min at a current density of 10 mA cm^{-2} to obtain *p*-type porous silicon. Zinc oxide nanoparticles were produced using a chemical precipitation method (CPM) and applied to (glass, PSi) substrates using (DCM). XRD and UV-Vis have also been used to study the properties of films (structural and optical). According to the XRD data, the ZnO NPs are wurtzite-structured polycrystalline, with a favored orientation along the (101) plane. The size of the ZnO NP crystals was measured by the Scherrer formula and the crystal size was found to be 22.04 nm. Images and distribution plots obtained using atomic force microscopy (AFM) indicated that the *p*-PSi had a particle size of approximately 47.22 nm and a porosity of (48 %). An ultraviolet (MS) detector based on porous (Si)/ZnO NPs (metal semiconductor) was fabricated at a temperature of (85 °C). The fabricated device showed a maximum detector photoresponse of 2.08 A/W at a wavelength of 450 nm at a bias voltage (+ 3.35 V). The factory-made UV ZnO detector has a normalized detection (D^*) of approximately (2.9×10^{13}) cm. 1/2 Hz/W at (λ = 450 nm). This approach provides an economical substrate and a facile synthetic method for optimizing the growth of *p*PSi/ZnO NPs, This has led to the successful fabrication of nanoscale photodetectors with potential applications for nanoscale photodetectors is displayed.

Keywords: *p*-PSi/ZnO, PCM, X-ray diffraction, ECE, UV-Photo detector.

1. INTRODUCTION

Ultra-Violet (UV) photoconductive finders have started a part of intrigued due to their wide assortment of employments. Natural observing, rocket discovery frameworks, and sun oriented space science are among the foremost well known applications [1, 2]. The silicon substance was secured the UV location region within the final decade. The destitute quantum productivity within the profound UV run due to the passivation layer is one of numerous noteworthy inadequacies of silicon bright photodetectors. The second limiting factor is the Si photodiode's age reduction when exposed to radiation with a significantly greater vitality than the Si band contrast [3]. ZnO may be a semiconductor with a wide and coordinate band gap that might be used in UV discovery [3, 4]. The UV finder built on a lean polycrystalline ZnO film contains a moo responsiveness and a long reaction time of a couple of minutes [5]. Then one dimensional ZnO NP are recognized via the presence of profound level layer trap states, for photo carriers within the ZnO locator have a long lifetime [7]. In spite of the truth that there has been a part of inquire about on ZnO UV locators, the larger part of it has centered on making strides the miniaturized scale cover terminals in arrange to extend the productivity of ZnO photoconductive locators [6]. The surface treatment of the ZnO lean film was utilized to extend the photo-responsivity of the ZnO UV finders. The productivity of the finder has been upgraded by coating the ZnO NP film surface howerver nano-sheets of different

sorts of polymers [7]. The photoconductive detector's photoresponsivity was expanded to around 2.24 A/W by coating the ZnO film surface with polyamide nylon, but the response time was as it were many seconds [8]. The lion's share of distributed inquire about on moving forward response time centers on the creation of photodiodes [14]. In this work, a basic and exceedingly dependable method is utilized to manufacture tall speed photoconductive ZnO UV locator of sensible photoresponsivity by keeping the ZnO NPs on *p*-PSi, can be made by electrochemical carving (ECE) with current thickness 10 mA·cm^{-2} and 10 min of time anode.

2. MATERIALS AND METHODS

2.1 Fabrication of Porous Silicon (PS)

The substrate was a (100) oriented p^+ (5 /cm², 500 μm) silicon plate (Bioanalyse, Turkey). First, it was washed twice with acetone and methanol in an ultrasonic bath. The surface was then etched using HF (42 percent) diluted 1:10 with distilled (DI) water to remove particles remaining on the silicon surface. Electrochemical etching of the silicon wafer surface produces porous silicon. Purified Si was placed on the bottom of the Teflon cell in a 1:1 ratio as opposed to a combination of HF (46 %) and 100 % ethanol. The electrode was a gold ring that was subjected to a 10 mA cm^{-2} current density for 10 minutes. Following nitrogen gas drying [9], the prod-

* dr.ahmed.alaskari89@gmail.com

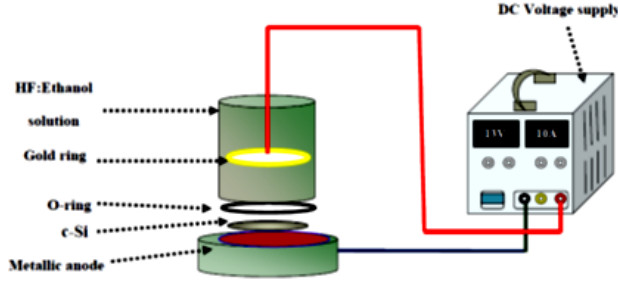uct is next submerged in distilled water containing porous silicon, as seen in Figure 1.

Fig. 1 – Schematic of an electrochemical etching setup

2.2 Preparation of Zinc Oxide Nanoparticles (ZnO NPs)

ZnO NPs were obtained by chemical vapor deposition. Precursors included zinc chloride ($ZnCl_2$) and sodium hydroxide (NaOH), and PVC was used as a stabilizer. (13.6) g of ($ZnCl_2$) solution (Central Drug House (P) India, 97.0 percent) was prepared using conventional processes in 100 ml of deionized water and heated at 75 °C. until completely dissolved. Hold on and become transparent. Appropriate amounts of NaOH (1 M) and 0.5 g of PVC (Sigma Aldrich USA, 99.9 %) were then used during normal processing. After allowing the solution to settle at the end of the reaction, the supernatant was decanted and purified with double distilled water and ethyl alcohol. The washing technique was repeated several times to remove remaining contaminants within the sample. The final white product was dried in a hot air oven (500 °C) for (1) h to form nano-sized ZnO powder particles.

2.3 Device Fabrication

Zinc oxide (ZnO) was connected in extent to permeable silicon (sort p) by drop casting (DCM) and warmed at a temperature of 85 °C and a thickness of (1.2) μm. The cover was utilized as an anode for the testimony of aluminum (99.9) % wires settled on the arranged film (ZnO), the aluminum anode was kept as an terminal by warm dissipation at a weight of 10 Dad and a thickness of 250 μm. it was done., a 10 mm^2 range on a ZnO/PSi/*p*-Si wafer. As a result, an Al/ZnO/p-PSi/Al photodetector as appeared in Fig. 1 was gotten 2.
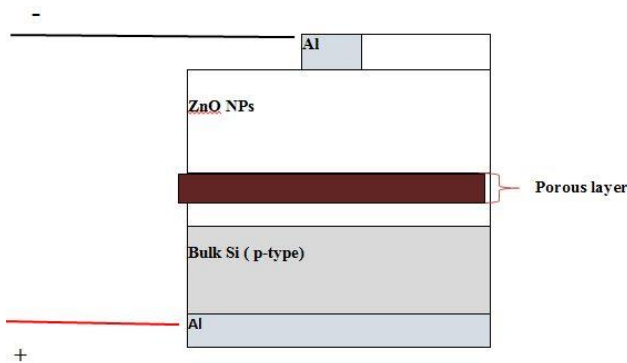

Fig. 2 – Structure of Al/ZnO/*p*-PSi/Al device design

2.4 Characterization

Diffraction designs and crystallite sizes of zinc oxide nanoparticles were measured employing a Shimadzu (6000.0) sort (Japan) X-ray diffractometer utilizing CuK radiation (wavelength = 1.5406 Å) (10°-80°) and measured. Calculate the precious stone volume (*D*) concurring to the connection [8-11] utilizing the Scherrer equation.

$$D = \frac{K\lambda}{\beta\cos\theta} \quad (1)$$

where K – constant, λ – X-ray wavelength, 0.154060 nm, β – full width at half maximum, θ – Bragg angle.

The optical absorption of thin films (ZnO) at room temperature was determined using a UV-VIS-NIR spectrophotometer (Shimadzu, UV-1800). The spectral structure of the response is investigated in the wavelength range (350-1000) nm with a shift of 3.35 eV, as in Eq. [11].

$$R_\lambda = \frac{I_{Ph}}{P_{in}}\left(\frac{A}{W}\right) \quad (2)$$

As I_{Ph} – the photo-current and P_{in} – the input power. Detection depends on the area of the detector and therefore on the power equivalent to the mutual noise of the detectors. To provide a 'quantum quality' factor based on the actual properties of the detector rather than the detector droplet size, we use a term called the allowable detection configuration [12].

$$D_\lambda = \frac{1}{NEP}\left(\frac{R_\lambda}{I_n}\right) \quad (3)$$

I_n – noise current and it can occaionaly be expressed as:

$$D_\lambda = \frac{S/N}{P_{in}} \quad (4)$$

S – the signal, N – the noise and P_{in} – the input power.

Detectivity is denoted by the symbol D_λ, which may be defined as the known *D*-star (NEP square value).

$$D^* = R_\lambda \frac{A^{\frac{1}{2}}\Delta f^{\frac{1}{2}}}{I_n} \quad (5)$$

$$I_n = \sqrt{2qI_d}\sqrt{\Delta f} \quad (6)$$

Δf – noise bandwidth. Since D_λ – is independent of detector area, directivity can measure the intrinsic quality of the detector material itself. When measuring the D_λ value of a photodetector, it is usually measured by a system that modulates or frequency-divides the incident light (*f*) to produce an AC signal and amplifies it to widen the bandwidth Δf. You must enter these quantities. The dependence of D_λ on wavelength (λ) and the sign of D_λ (λ, *f*, Δf) can describe the frequency and bandwidth over which measurements are made. Therefore, this is often the reference bandwidth (1 Hz). The unit D_λ (λ, *f*, Δf) describes a detector suitable for detecting weak

signals in the presence of noise [13]. An important parameter of the photodetector is the detection wire when the detectable power is low. So the width of the detector is similar to this parameter. Using the composite charge approximation, the change in carrier excess charge (lifetime) with diode size can be expressed by Equation [14].

$$\tau = \frac{1}{f}, \qquad (7)$$

where τ – is Carrier lifetime, f – frequency.

3. RESULTS

3.1 Structural Analysis

In the diagram. Figure 3 shows the X-ray diffraction pattern of the synthesized crystal (ZnO nanoparticles). Figures 1-3 show the X-ray diffraction patterns of ZnO thin films. (3). From Figure (3), [(100), (002), (101) and (102), (110), (103), (112) and (201)] are preferred destinations respectively, and JCPDS card numbers [0036-1451] and other reports [15]. Table No. (1) shows the preferred direction. Diffraction peaks of the pristine thin film indicate the hexagonal structure of wurtzite. As a result of the XRD data, the films obtained in this study consist entirely of a pure (ZnO) phase with no secondary phases. The lattice constants ($a = b = 0.3253$ nm) and ($c = 0.5217$ nm) of ZnO were determined. Both numbers are close to the theoretical values ($a = b = 0.3249$ nm) and ($c = 0.5206$ nm), and other studies [16, 17] used Scherrer's equation (1) to estimate the crystal size (D).
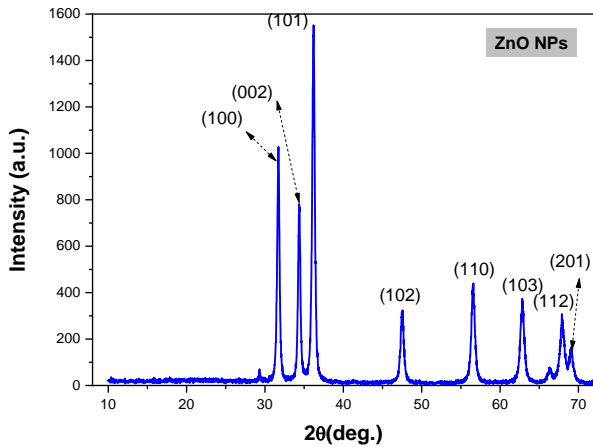

Fig. 3 – XRD patterns of ZnO thin films at 500 °C annealing temperatures

On the diagram a shows crystalline silicon (c-Si) (p-type) by X-ray diffraction (XRD). Moreover, the figure shows that the c-Si peak has higher intensity and extension value than the PSi peak. On the diagram Fig. 4b shows a p-type X-ray diffraction (XRD) PSi layer. The single crystal structure of the p-type P_{Si} layer is (($2\theta \sim 69.428°$)) direction (400) only. This model refers to the reflecting surface of the Si (400) cubic structure (according to JCPDS) [16]. X-ray diffraction of nanocrystals on the pore walls is responsible for this effect. As shown in this figure, the P_{Si} layer is still crystallized.
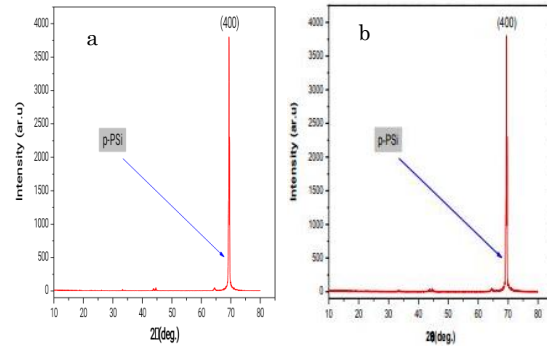

Fig. 4 – XRD pattern of crystalline silicon (c-Si) and PSi sample etching current density for (10.0 mA/cm² and anodized 10 min/ etching time of p-type

Table 1 – Structural parameters of (ZnO NPs)

Structural parameters	Zinc oxide (ZnO)	
2θ (deg)	36.199	
hkl	(101)	
d (Å)	2.479	
(FWHM) (rad)	0.0066	
(D) (nm)	22.04	
Lattice Constants (nm)	a=b	0.3253
	c	0.5217

3.2 Porous Silicon Investigated with AFM (P_{Si})

AFM images are presented in this section to investigate the structural properties and porosity of PSi. Figure 5 shows a 3D plot of the distribution of oxide precipitates (p-P_{Si}) and particles at an etching time of 10 min and a current density of 10 mA/cm2. was used to determine the average. The particle size (Gs) of P_{Si} (p-type) was found to be (47.22 nm), as shown in Table 2. AFM tests showed that the surface morphology of the P_{Si} (p-type) layer was very smooth and uniform, and that the film consisted of an array of randomly arranged columns of nanocrystalline silicon in the same direction. rice field.
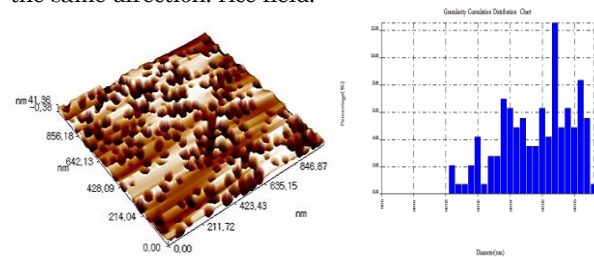

Fig. 5 – P_{Si} granularity accumulation distribution chart and (3D AFM) surface images (p-type)

Table 2 – The average grain size, roughness average, Root mean square and porosity of n-type P_{Si}

p-P_{Si}	Average grain size (nm)	RMS (nm)	Surface roughness (nm)	Porosity %
	47.22	10.7	12.3	0.48

3.3 Optical Absorbance

In the diagram (6) shows the absorption spectrum of the ZnO film. This is very important as it provides detail in the optical range and gradually increases at higher energies in the range (λ = 223-328 nm). This apparent drawback is related to the interaction between electrons in the material and incident photons with sufficient energy to carry out electronic transitions.
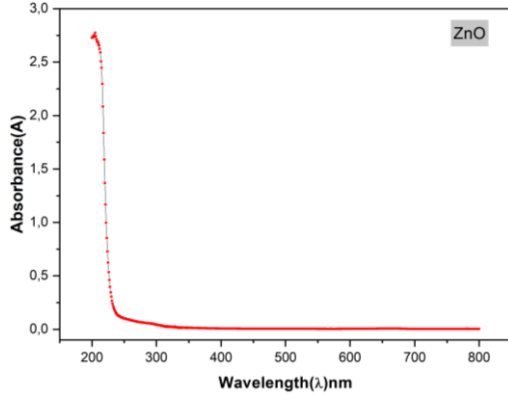

Fig. 6 – The absorbance of ZnO thin film as a function of wavelength

3.4 Detector Performance Parameters Measurement

Spectral Responsivity (R_λ)

Figure (7) shows the spectral response as a function of the wavelength within the range (350-1000) nm with bias voltage (3.35 V) and it is computed through equation (2). The curve of spectral responsivity (R_λ) for ZnO/p-Porous Silicon has two peaks, as seen in the figure; the "first peak" at a wavelength of (450) nm which corresponds to almost with the cutoff wavelength of ZnO film, while the "second peak" is located at (λ = 850 nm) because of silicon's absorption edge, the reason for the increased response at 350 nm with increasing wavelength is the films' surface-level absorption of short wavelengths, which has a high absorption factor at those wavelengths and causes a gradual rise in the spectral response. By analyzing the spectral response, it is possible to determine the response for heterojunctions (2.08)A/W, which is what has been documented in the literature [18]. front lighting with a bias of + 3.35 V. The created p-P$_{Si}$/ZnO NPs device has a high UV sensitivity, quick reaction, and high responsiveness. The high length-to-diameter and crystallinity of p-P$_{Si}$/ZnO may be the cause of these exceptional properties.

Specific Detectivity (D^*)

The specific detectivity is defined as one of the important parameters for photodetector which represents the minimum detectable power, therefore the performance of the detector is linked with this parameter, which defines the efficiency and the optimal application region (Wavelength). The value of the specific detectivity is determined by noise from surrounding radiation, Johnson -noise, noise generated by the random movement of electrons and holes,
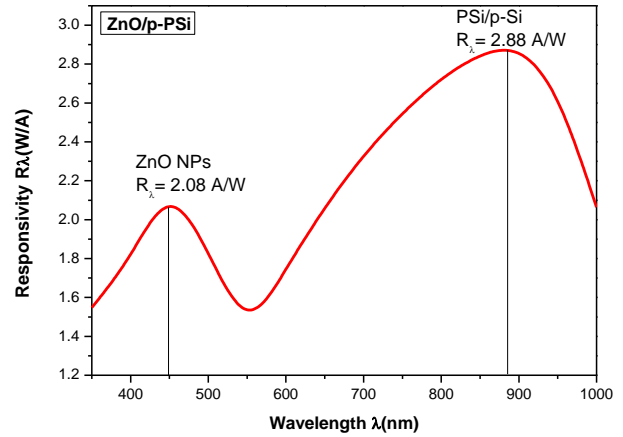

Fig. 7 – The variation of spectral responsivity with wavelength for ZnO/PSi/p-Si

transit time, and noise diverse. As shown in Figure (8) the (D^*) is a function of λ for Photo-detectors manufactured. That the curve behaves similarly to spectral response behavior because the value of the specific detectivity is dependent on the spectral response according by relationship (3 & 5). It has been observed that the specific detectivity is greater than (10^{10} cm·Hz$^{1/2}$/W), thus, the heterojunction is workable. From the Figures, the detectivity D^* for heterojunctions found (2.9×10^{13}) cm·Hz$^{1/2}$/W at (λ = 450 nm) for ZnO/p-P$_{Si}$ Photodetector, ZnO nanoparticles exhibit (λ_{exc} = 450 nm) sharp UV band corresponding to near band gap excitonic emission and broad green emission band due to the oxygen vacancy at room temperature.
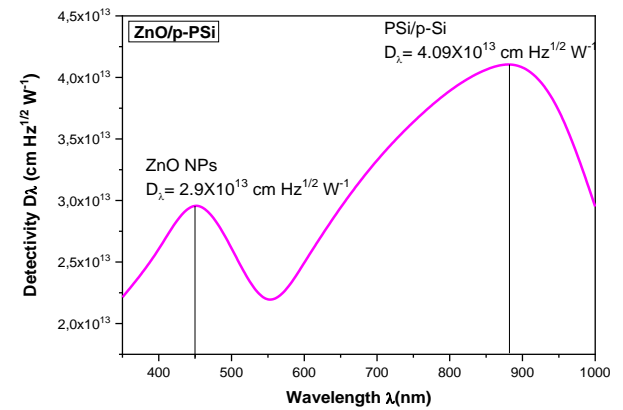

Fig. 8 – The variation of spectral detectivity with wavelength for ZnO/PSi/p-Si

Minority Carrie Life Time (MCT) Measurement

Carrier mobility (μ) can be perfectly visualized and is therefore considered an important parameter for heterogeneous bonding. MCT (τ Life) is the average time between carrier generation and recombination as it determines the efficiency of many semiconductor devices such as photodetectors [10]. Figure (9) represents the charge carrier lifetime, which describes the recombination process in a semiconductor device and is calculated by equation (7). An indicator that the transit times are consistent with the fact that no recombination has oc-

curred improved the performance of the device after introducing pre-trained NPs in (P$_{Si}$). The photodetector was obtained with a lifetime (5.65 ms). This usually means that bulk-generated minority carriers persist for a long time before recombination. This indicates a reduced recombination probability. In general; the lifetime (τ Life) of an electron in a semiconductor is 10^{-8} seconds. The response time was set short (2.6×10^{-5}) seconds.

Fig. 9 – The lifetime measurements of charge carriers by open-circuit voltage decay photograph method for ZnO/PSi/*p*-Si

4. CONCLUSIONS

In this study, ZnO NPs were successfully obtained and deposited on substrates (glass and porous silicon) by drop casting. The X-ray diffraction patterns of ZnO and p-PSi NPs show that the films (polycrystalline and monocrystalline) are crystalline with wurtzite structure and cubic hexagonal structure, respectively. The main peak characteristics are assigned to the (101) and (400) planes respectively. Porous silicon was successfully obtained from silicon wafers (p^+) by electrochemical etching. A thin ZnO film was successfully deposited on porous silicon by drop casting. Judging from the absorption spectra, the deposition of ZnO NPS on P$_{Si}$ exhibited the properties of porous photodetectors. A ZnO/P$_{Si}$/*p*-Si/Al(R_λ) photodetector was found to have (2.88 A/W) at ($\lambda = 885$ nm) due to the absorption edges of silicon and porous silicon. This was approximately (2.08 A/W) at $\lambda = 450$ nm due to the absorption edge of the ZnO NPS. The highest qualitative detection value (D_λ) was (2.9×10^{13}) cm$^{1/2}$ W^{-1} Hz at ($\lambda = 450$ nm) and (4.09) cm$^{1/2}$ W^{-1} Hz at ($\lambda = 885$ nm). Al/ZnO/P$_{Si}$/*p*-Si/Al photodetector.

REFERENCES

1. L. Luo, Y.F. Zhang, S.S. Mao, L.W. Lin, *Sensor. Actuator. A Phys.* **127** No 2, 201 (2006).
2. E. Monroy, F. Omnes, F. Calle, *Semicond. Sci. Technol.* **18** No 4, 33 (2003).
3. A. Müller, G. Konstantinidis, M. Dragoman, D. Neculoiu, A. Dinescu, M. Androulidaki, M. Kayambaki, A. Stavrinidis, D. Dascalu, A. Kostopoulos, *Appl. Opt.* **47**, 1453 (2008).
4. S.J. Young, L.W. Ji, S.J. Chang, Y.K. Su, *J. Cryst. Growth.* **293** No 1, 43 (2006).
5. X.G. Zheng, Q.S. Li, J.P. Zhao, D. Chen, B. Zhao, Y.J. Yang, L.C. Zhang, *Appl. Surf. Sci.* **253** No 4, 2264 (2006).
6. Q.A. Xu, J.W. Zhang, K.R. Ju, X.D. Yang, X. Hou, *J. Cryst. Growth* **289** No 1, 44 (2006).
7. I.K. Abd, A.M. Shano, E.K. Alwan, *J. Nano- Electron. Phys.* **14** No 6, 06002 (2022).
8. I.K. Abd, A.M. Shano, E.K. Alwan, *J. Nano- Electron. Phys.* **14** No 3, 03024 (2022).
9. Z.T. Khodiar, N.F. Habubi, A.K. Abd, A.M. Shano, *Int. J. Nanoelectron. Mater.* **13** No 3, 433 (2020).
10. M. Ali, A. M. Shano, N.A. Bakr, *J. Mater. Sci.: Mater. Electron. Mater.* **29** No 13, 11208 (2018).
11. A.M. Shano, Z.S. Ali, *J. Nano- Electron. Phys.* **12** No 4, 04001 (2020).
12. A.M. Shano, R.A. Ali, Z.T. Khodair, S.K. Adnan, *AIP Conf. Proc.* **2475** No 1, 09007 (2023).
13. M. Shano, A.M. Khudhur, A.S.H. Abbas, N.B. Bakr, I.M. Ali, *IOP Conf. Ser. Earth Environ. Sci.* **790** No 1, 012085 (2021).
14. M.K. Trivedi, R.M. Tallapragada, A. Branton, D. Trivedi, G. Nayak, O. Latiya, S. Jana, *J. Adv. Chem. Eng.* **5** No 4, 1000136 (2015).
15. L. Fadillah, B. Soegijono, S. Budiawanti, I. Mudzakir, *AIP Conf Proc.* **1862**, 030053 (2017).
16. Z.M. Khoshhesab, M. Sarfaraz, M.A. Asadabadm, *Inorg. Nano-Met. Chem.* **41**, 814 (2011).
17. A.M. Shano, S.A. Khadhir, A.A. Mohammed, S.K. Adnan, O.A. Ahmed, *AIP Conf. Proc.* **2834**, 090023 (2023).
18. A.A. Thahe, H. Bakhtiar, A.A. Basant, Z. Hassan, N. Bidin, M. Bououdina, M.A. Qaeed, Z.A. Talib, Mohammed A. Al-Azawi, Hasan Alqaraghuli, M.B. Uday, A. Ramizy, M.S. Al-Ghamdi, D. Abubakar, N.K. Allam, *Opt. Mater.* **84**, 830 (2018).

Полікристали оксиду цинку для гетеропереходу та інфрачервоний УФ-фотодетектор

Saif Khalel Jasim[1,2], Ahmed M. Shano[2], Suzan K. Adnan[1]

[1] *Ministry of Education, Diyala Education Directorate, Diyala, Iraq*
[2] *Department of Radiological Tech., Bilad Alrafidain University College, 32001 Diyala, Iraq*

У даній роботі було використано електрохімічне травлення кремнієвих пластин *p*-типу протягом 10 хвилин при густині струму 10 mA cm^{-2} для отримання пористого кремнію *p*-типу. Наночастинки оксиду цинку були виготовлені за допомогою методу хімічного осадження (CPM) і нанесені на (скло,

PSi) підкладки за допомогою (DCM). XRD і UV-Vis також використовувалися для вивчення властивостей плівок (структурних і оптичних). Згідно з даними XRD, НЧ ZnO є полікристалічними з вюрцитною структурою, з вигідною орієнтацією вздовж площини (101). Розмір кристалів ZnO NP вимірювали за формулою Шеррера, і було встановлено, що розмір кристала становить 22,04 нм. Зображення та графіки розподілу, отримані за допомогою атомно-силової мікроскопії (АСМ), показали, що p-PSi має розмір частинок приблизно 47,22 нм і пористість (48 %). Ультрафіолетовий (MS) детектор на основі пористих (Si)/ZnO НЧ (металевий напівпровідник) був виготовлений при температурі (85 °C). Виготовлений пристрій продемонстрував максимальний фотовідповідь детектора 2,08 А/Вт на довжині хвилі 450 нм при напрузі зміщення (+ 3,35 В). Виготовлений на заводі УФ-детектор ZnO має нормалізоване виявлення (D^*) приблизно (2.9×10^{13}) см. 1/2 Гц/Вт при ($\lambda = 450$ нм). Цей підхід забезпечує економічну підкладку та легкий синтетичний метод для оптимізації росту наночастинок pPSi/ZnO. Це призвело до успішного виготовлення нанорозмірних фотодетекторів із потенційним застосуванням для нанорозмірних фотодетекторів. відображається.

Ключові слова: p-PSi/ZnO, PCM, X-ray дифракція, ECE, UV-фотодетектор.